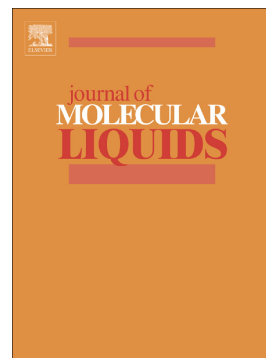


Accepted Manuscript

Understanding corrosion inhibition of mild steel in acid medium by new benzonitriles: Insights from experimental and computational studies

A. Chaouiki, H. Lgaz, Ill-Min Chung, I.H. Ali, S.L. Gaonkar, K.S. Bhat, R. Salghi, H. Oudda, M.I. Khan



PII: S0167-7322(18)31285-6
DOI: doi:[10.1016/j.molliq.2018.06.103](https://doi.org/10.1016/j.molliq.2018.06.103)
Reference: MOLLIQ 9301
To appear in: *Journal of Molecular Liquids*
Received date: 12 March 2018
Revised date: 14 May 2018
Accepted date: 26 June 2018

Please cite this article as: A. Chaouiki, H. Lgaz, Ill-Min Chung, I.H. Ali, S.L. Gaonkar, K.S. Bhat, R. Salghi, H. Oudda, M.I. Khan , Understanding corrosion inhibition of mild steel in acid medium by new benzonitriles: Insights from experimental and computational studies. Molliq (2018), doi:[10.1016/j.molliq.2018.06.103](https://doi.org/10.1016/j.molliq.2018.06.103)

This is a PDF file of an unedited manuscript that has been accepted for publication. As a service to our customers we are providing this early version of the manuscript. The manuscript will undergo copyediting, typesetting, and review of the resulting proof before it is published in its final form. Please note that during the production process errors may be discovered which could affect the content, and all legal disclaimers that apply to the journal pertain.

Understanding Corrosion Inhibition of Mild Steel in Acid Medium by new Benzonitriles: Insights from Experimental and Computational Studies

A. Chaouiki^{1,2}, H. Lgaz^{3*}, Ill-Min Chung^{3*}, I. H. Ali⁴, S. L. Gaonkar⁵, K. S. Bhat⁵, R. Salghi^{2*}, H. Oudda¹ and M. I. Khan⁶

¹Laboratory separation processes, Faculty of Science, University Ibn Tofail PO Box 242, Kenitra, Morocco

²Laboratory of Applied Chemistry and Environment, ENSA, University Ibn Zohr, PO Box 1136, Agadir, Morocco

³Department of Applied Bioscience, College of Life & Environment Science, Konkuk University, 120Neungdong-ro, Gwangjin-gu, Seoul 05029, South Korea

⁴Department of Chemistry, College of Science, King Khalid University, P. O. Box 9004, Postal Code 61413, Saudi Arabia

⁵Department of Chemistry, Manipal Institute of Technology, Manipal Academy of Higher Education, Manipal, Karnataka, India

⁶Chemical Engineering Department, College of Engineering, King Khalid University, Abha, Kingdom of Saudi Arabia

*Corresponding Authors:

E-mail addresses: r.salghi@uiz.ac.ma (R. Salghi), lgaz.hassan@gmail.com (H. Lgaz), imcim@konkuk.ac.kr (Ill-Min Chung).

ABSTRACT

Two benzonitrile derivatives, namely 4-(isopentylamino)-3-nitrobenzonitrile (PANB) and 3-amino-4-(isopentylamino)benzonitrile (APAB) have been synthesized and evaluated as corrosion inhibitors for mild steel (MS) in 1 M HCl solution at 303K by gravimetric, potentiodynamic polarization (PDP) curves, and electrochemical impedance spectroscopy (EIS) methods, as well as Density Functional Theory (DFT) and Molecular Dynamic (MD) simulations. The results suggest that tested compounds are excellent corrosion inhibitors for mild steel with PANB showing superior performance. Polarization measurements revealed that PANB and APAB behaved as mixed type inhibitors. The polarization resistance, according to EIS studies, found to be dependent on the inhibitor's concentration. The adsorption of PANB

and APAB on mild steel surface obeyed Langmuir's adsorption isotherm. On the one hand, DFT and MD simulations are being used to explain the effect of the molecular structure on the corrosion inhibition efficiency and on the other hand to simulate the adsorption of benzonitrile derivatives on mild steel surface. The protection of carbon steel in 1 M HCl was confirmed by using scanning electron microscope (SEM) and Atomic Force Microscopy (AFM). Electrochemical, DFT and MD simulations results are in good agreement.

Keywords: Benzonitrile derivatives; Corrosion inhibition; Mild steel; Acid solutions; DFT; MD simulations.

1. Introduction

Hydrochloric acid is a strong inorganic acid that is extensively used in many industries, like oil, gas and chemical industries. Unlike many other metals, mild steel is the most commonly-used material in these industries; it came to be used for most purposes where wrought iron was formerly used[1,2]. Nonetheless, the major problem associated with its use seems to reach its high susceptibility to corrosion in acidic solutions, which results in a considerable loss in its essential properties. In order to adopt effective preventive methods against corrosion of metals, various strategies have been applied to control this undesirable phenomenon such as materials selection, cathodic protection, coatings and the use of corrosion inhibitors. The inhibitors have been considered as the most practical and easiest method. Typically, these organic compounds along with heteroatoms and lone pair have shown good inhibition performance for many metals and rapid progress in recent years has been made in the design and synthesis of a variety of compounds such as quinoles, quinoxalines, pyridinium, triazoles and imidazolines...etc[3]. They seem to act by adsorbing onto the surface of metal, blocking one or more of the undesirable reactions occurring at the solution/metal interface and therefore causing high protection of metal against dissolution[4,5]. Benzonitriles and related compounds having nitrile group as the substituent are known corrosion inhibitors. For example, a novel azo nitrile derivative reported as an effective inhibitor of corrosion copper in nitric acid medium [6]. Here, the structure of the inhibitors contains an additional azo group in addition to the nitrile group. Simple aliphatic and aromatic nitrile compounds have been investigated for their inhibitive action and found that effective in reducing hydrogen embrittlement on steel surface[7,8].

In recent years, to understand some unknown properties during the interaction of inhibitors with the metal surfaces, theoretical chemistry and molecular simulation studies have been used in

this context. Density Functional Theory based calculations have been proved to be a very powerful tool for studying the electronic and structural properties of inhibitors. The geometry of the inhibitor molecule in its ground state and the nature of their molecular orbitals (HOMO; Highest Occupied Molecular Orbital and LUMO; Lowest Unoccupied Molecular Orbital) are directly involved in the inhibitive properties of these molecules. Such calculations, though instructive, are not always adequate for providing more clarification of the experimental results. Modeling of an experiment by molecular dynamic (MD) simulations has been accepted as an effective and authentic technique. MD simulations are particularly well-poised to investigate the structure of the corrosion inhibitors and the mechanism of inhibition at an atomic level under a variety of conditions[9].

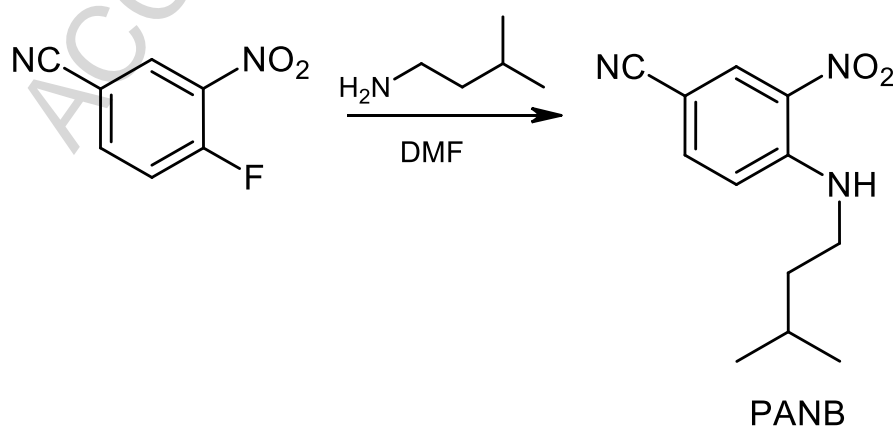
In this contribution, weight loss measurements, potentiodynamic polarization and electrochemical impedance spectroscopy have been successfully used for the analysis of the anti-corrosive efficiency of novel benzonitrile derivatives in 1.0 M HCl. Meanwhile, MD simulations and DFT calculations were carried out to explain the proposed inhibition mechanism between the inhibitor and metal surface. These inhibitors are having structural similarity, only differing in the nature of substituent groups attached with the phenyl. MS samples were further studied by scanning electron and atomic force microscopies.

2. Materials and methods

2.1. Synthesis of inhibitors

General procedure for the Synthesis of novel benzonitrile derivatives is given below:

❖ Synthesis of compound 4-(isopentylamino)-3-nitrobenzonitrile (PANB):

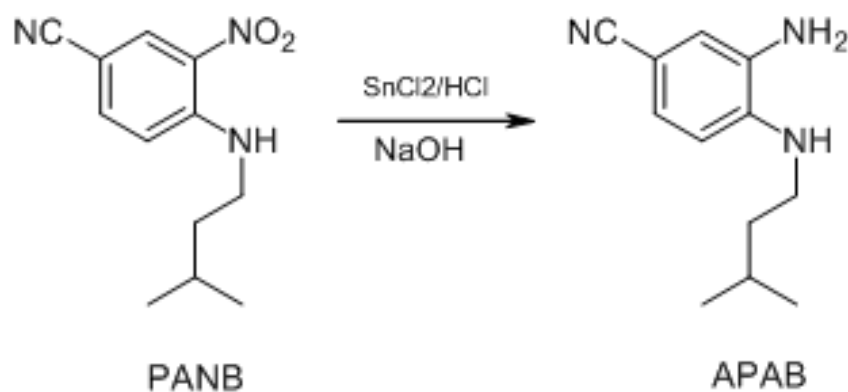


Scheme 1.Preparation of 4-(isopentylamino)-3-nitrobenzonitrile (PANB)

A stirred solution of 4-fluoro-3-nitrobenzotrile (14.97 g, 9 mmol) in MeCN (15 mL) was placed under an N₂ atmosphere. Isopentylamine (1.58 g, 18 mmol) was added dropwise at rt for a period of 30 min. The reaction mixture was stirred at room temperature for 1 hour after which it was poured on water (60 mL) and stirred for 15 minutes. The resulting solid was collected, washed with water (2 x 20 mL). The solid was dried in a vacuum oven at 40 °C to give 4-(isopentylamino)-3-nitrobenzotrile (PANB) (2.06 g, 98%) as a yellow solid.

¹H NMR (400 MHz, DMSO-d₆) δ ppm: 1.01(d, 2H, 2X-CH₃), 1.60-1.69 (m, 3H, -CH and -CH₂), 3.4 (t, 2H, -CH₂), 4.1 (s, 1H, -NH), 7.28-7.33 (m, 5H, ArH), 7.38 (d, 2H, ArH), 7.45 (d, 2H, ArH). ¹³C NMR (100 MHz, DMSO-d₆) δ ppm: 23.1, 25.9, 39.9, 41.5, 101.2, 115.9, 118.9, 130.1, 135.0, 139.2, 149.8.

❖ **Synthesis of compound 3-amino-4-(isopentylamino)benzotrile (APAB):**



Scheme 2. Preparation of 3-amino-4-(isopentylamino)benzotrile (APAB).

A three neck RBF was charged with of Hydrochloric acid (10 mL), SnCl₂ (1.6 g, 8.5 mmol). Under stirring 4-(isopentylamino)-3-nitrobenzotrile (PANB) (1.0 g, 4.2 mmol) was added for a period of 30 min. The reaction mixture was stirred for 1 hour. The mixture was diluted with water (10 mL) and basified with dilute NaOH. The solid formed was filtered and crystalized from ethanol to give 3-amino-4-(isopentylamino)benzotrile(APAB) as a brown solid to yield (0.80 g, 91 %).

¹H NMR (400 MHz, DMSO-d₆) δ ppm: 1.02 (d, 6H, 2X -CH₃), 1.60-1.68 (m, 3H, -CH and -CH₂), 3.42 (t, 2H, -CH₂), 4.1 (s, 1H, -NH), 6.41 (s, 2H, -NH₂), 6.60 (s, 1H, ArH), 6.64 (d, 1H, ArH), 6.81 (d, 1H, ArH). ¹³C NMR (100 MHz, DMSO-d₆) δ ppm: 23.2, 25.9, 40.1, 42.8, 101.1, 115.9, 115.3, 118.4, 121.9, 123.1, 134.4, 140.8.

2.2. Materials and corrosive solutions

The coupons used for the corrosion tests were made of mild steel with a chemical composition of: 0.370 % C, 0.230 % Si, 0.680 % Mn, 0.016 % S, 0.077 % Cr, 0.011 % Ti, 0.059 % Ni, 0.009 % Co, 0.160 % Cu, and balance Fe. Prior to each individual experiment, test coupons were mechanically abraded using a belt grinding polishing machine. To obtain a polished surface, MS surface was grounded with emery papers of decreasing grit size from 600 to 1600 grades. Afterwards, the samples were rinsed with distilled water, degreased in ethanol and dried in warm air prior to use. The test solution (1 M HCl) was prepared from the reagent grade 37% HCl and distilled water. Solutions of the inhibitors in 1 M HCl were prepared to obtain different concentrations range of 1×10^{-4} M to 5×10^{-3} M at 303 K. The organic compounds tested were PANB and APAB and are given in Figure 1.

2.3. Electrochemical measurements

Electrochemical measurements were conducted in an 80 mL three-electrode cell assembly with a working electrode (mild steel, 1 cm² dimension), platinum as auxiliary electrode and saturated calomel as reference electrode (SCE) placed in a constant temperature bath. All potentials within the text are referred to the SCE. Electrochemical experiments were performed on a Volta lab PGZ 100 Instrument with a Volta master 4.0 software package for experimental applications. The results were fitted using EC-Lab software package. All electrochemical tests were performed after 30 minutes at the temperature of 303K. Electrochemical impedance spectroscopy (EIS) measurements were conducted over a frequency range of 100 KHz – 10 mHz with signal amplitude perturbation of 5 mV. Potentiodynamic polarization experiments were carried out at the scan rate of 1 mV/s over the potential range from -800 to -200mV/SCE. All experiments were run in triplicate to confirm the reproducibility.

2.4. Weight loss measurements

According to the ASTM standard [10], disk-shaped specimens (38 mm in diameter and 3 mm in thickness with a hole of 8 mm diameter) were prepared for each weight loss test. The mild steel samples were immersed in uninhibited and inhibited solutions for 6h at 303K. The MS samples were prepared as mentioned previously and weighted using a precision balance with a sensitivity of 0.1 mg. After each test, the MS specimens were taken out and rinsed thoroughly

with distilled water and acetone, dried and weighted accurately again. The following equation (Eq. (1)) was used to determine the corrosion rate in millimeters per year (mm y^{-1}):

$$C_{RW} = \frac{K \times W}{A \times t \times \rho} \quad (1)$$

Where $K = 8.76 \times 10^4$ was used as a constant. W and t are the mass loss in gram and the time of exposure in hours. According to ASTM G1-03 standard[11], the density of mild steel is 7.86 g cm^{-3} . The exposed area, A (in cm^2) was calculated from Equation (2)[12]:

$$A = \frac{\pi}{2} (D^2 - d^2) + l\pi D + l\pi d \quad (2)$$

Where D , d and l are the diameter of mild steel pieces, the diameter of the hole for holding and the thickness, respectively. The following equations were used to calculate the inhibition efficiency η_{WL} (%) and the surface coverage (θ)[13]:

$$\eta_{WL} (\%) = \left[\frac{C_{RW}^{\circ} - C_{RW}}{C_{RW}^{\circ}} \right] \times 100 \quad (3)$$

$$\theta = \left[\frac{C_{RW}^{\circ} - C_{RW}}{C_{RW}^{\circ}} \right] \quad (4)$$

Where C_{RW}° and C_{RW} are the corrosion rates without and with various concentrations of the inhibitors, respectively, θ is the degree of surface coverage of tested inhibitors.

2.5. Theoretical calculations

Our current understanding of electronic properties of many corrosion inhibitors has been shaped by multiple theoretical studies[10]. The energy geometry optimization, quantum chemical parameters and Fukui functions were obtained using Gaussian program package, module version 9.0[10]. The calculations started without any geometry constraints until full geometry optimizations. The calculation was performed using higher basis set denoted by 6-311G++ (d,p)[11,14]. All quantum calculations were carried out in aqueous phase using Self-Consistent Reaction Field (SCRF) theory, with Polarized Continuum Model (PCM)[9]. The ionization energy and the electronic affinity were determined by the values of the energies of the HOMO and LUMO orbital[15]:

$$IP = -E_{\text{HOMO}} \quad (5)$$

$$EA = -E_{\text{LUMO}} \quad (6)$$

Then, electronegativity (χ) and chemical hardness (η) were evaluated, based on the finite difference approximation, as linear combinations of the calculated IP and EA:

$$\chi = \frac{IP + EA}{2} \quad (7)$$

$$\eta = \frac{IP - EA}{2} \quad (8)$$

The fraction of electrons transferred (ΔN) from inhibitor to metallic surface was calculated using the equation[16,17]:

$$\Delta N = \frac{\phi - \chi_{inh}}{2(\eta_{Fe} + \eta_{inh})} \quad (9)$$

Where ϕ is the work function used as the appropriate measure of electronegativity of iron, and $\eta_{Fe} = 0$. The value of $\phi = 4.82$ eV for Fe (110) surface which is reported to have higher stabilization energy[10,18].

The local reactivity of inhibitor molecules (nucleophilic and electrophilic attacks) were obtained by condensed Fukui functions[19], using the following equations[13]:

$$f_k^+ = q_k(N+1) - q_k(N) \quad (10)$$

$$f_k^- = q_k(N) - q_k(N-1) \quad (11)$$

Where $q_k(N)$, $q_k(N+1)$ and $q_k(N-1)$ represent charge values of atom k for neutral, anion and cation, respectively.

In all molecular modeling and simulation procedures, molecular dynamics (MD) simulation were carried out using Materials studio package[13] in a 10 x 10 super cell using the COMPASS force field with a time step of 1 fs, NVT ensemble and simulation time of 2000 ps[13] in a simulation box of $(24.82 \times 24.82 \times 35.69 \text{ \AA}^3)$. The Temperature was fixed at 303 K. The binding and interactions energies were estimated by using following Equations[20]:

$$E_{interaction} = E_{total} - (E_{surface+solution} + E_{inhibitor}) \quad (12) \text{ and } E_{Binding} = -E_{interaction} \quad (13)$$

Where E_{total} is the total energy of the entire system, $E_{surface+solution}$ refers to the total energy of Fe (110) surface and solution without the inhibitor and $E_{inhibitor}$ represents the total energy of the inhibitor. The calculations of Radial Distribution Function (RDF) were performed after MD simulations, the RDF, $g(r)$, is defined as the probability of finding particle B within the range $r + dr$ around particle A. RDF is defined as follows[21]:

$$g_{AB}(r) = \frac{1}{\langle \rho_B \rangle_{local}} \times \frac{1}{N_A} \sum_{i \in A} \sum_{j \in B} \frac{\delta(r_{ij} - r)}{4\pi r^2} \quad (14)$$

Where $\rho_{B \text{ local}}$ represents the particle density of B averaged over all shells around particle A .

2.6. Surface characterization

For SEM analysis, coupons were prepared following identical procedure as described for weight loss. The surface was immersed for 6 h in 1 M HCl solution prepared without and with the addition of optimum concentration of inhibitor at 303K. After 6 h the coupons were taken out, and thoroughly cleaned with distilled water, air-dried and subjected to SEM analysis. Atomic Force Microscopy (AFM) measurements were carried out using VEECO CPM to observe the surface roughness over time in the absence and presence of inhibitors.

3. Results and discussion

3.1. Potentiodynamic polarization studies

To pool information concerning the kinetics of anodic and cathodic reaction, the addition effect of both compounds at various concentrations in the aggressive electrolyte was investigated by polarization method. The curves obtained are shown in Figure 2. Extracted electrochemical parameters like corrosion current density (i_{corr}) and Tafel slopes (β_c and β_a), obtained from these graphs by extrapolation method are listed in Table 1. The corrosion inhibition efficiency $\eta_{\text{PDP}}(\%)$ was calculated using the relation[21]:

$$\eta_{\text{PDP}}(\%) = \left[1 - \frac{i_{\text{corr}}}{i_{\text{corr}}^{\circ}} \right] \times 100 \quad (15)$$

Where i_{corr} and i_{corr}° are the corrosion current density in the inhibited and uninhibited acid respectively. The percentage of inhibition efficiencies $\eta_{\text{PDP}}(\%)$ derived from equation (15) are also listed in Table 1.

From the Figure 2, we notice that in the presence of the inhibitors, the shapes of polarization curves have no distinct changes compared to the blank one with a prominent decrease in corrosion rate, which manifests the reaction mechanism of corrosion resistance process was not changed for studied inhibitors. Interestingly, the results revealed that both anodic and cathodic curves are being affected in the presence of both inhibitors suggesting that investigated compounds retard the anodic metal dissolution as well as cathodic hydrogen evolution reactions. The corrosion potential (E_{corr}) does not change significantly in presence of both

inhibitors, thus, the inhibitor molecules can be classified as mixed-type inhibitors, which implies the inhibitors reduce the anodic mild steel dissolution and also retards the cathodic hydrogen evolution reaction[22]. Upon inspection of Figure 2, it can be seen that when the potential goes towards positive values ~ -300 mV, the anodic branch a slightly changed. This result is well known as 'desorption potential' and it is consistent with other research which found that an increase in anodic currents is mainly associated with desorption potential that alters significantly the inhibitor film[23].

Results summarized in Table 1 indicate that, the current density values diminish in the order of PANB<APAB and a more prominent decrease was observed at higher inhibitor concentration which is attributable to the enhanced effectiveness in blocking the cathodic and anodic reaction sites at higher concentration and thereby hindering the electrochemical reactions occurring at those sites. Hence, we can infer that this phenomenon is due to the adsorption of the inhibitor molecules on steel surface leading to the increase of the surface coverage. Evidently, the inhibition efficiency reaches 95.42 and 93.86 at 5×10^{-3} M of PANB and APAB, respectively, which indicates that the $-\text{NO}_2$ substituted PANB has better blocking ability than that of the $-\text{NH}_2$ substituted inhibitor.

3.2. Electrochemical Impedance Spectroscopy measurements

In this paper, the electrochemical behavior at the interface of the mild steel in the free acid solution and the inhibited solution was described by EIS measurements. Figure 3 compares the Nyquist plots for mild steel immersed for 30 min without and with different concentrations of PANB and APAB. The EIS data recorded at the open-circuit potential illustrate a capacitive loop in form of depressed semicircles. That is to say that the charge transfer process mainly controls the dissolution of mild steel in 1 M HCl solution[24]. Furthermore, the diameter of the impedance spectra in presence of benzonitrile derivatives is much higher than that in the uninhibited solution, and this increase became more pronounced as inhibitor concentration increased, which suggests that the two studied inhibitors adsorbed on the metal surface and a protective film is formed[25,26]. Using the EC-Lab software, the electrical equivalent circuit illustrated in Figure 4[27] was used for analyzing the impedance spectra for the corrosion of MS. The equivalent circuit comprises of the solution resistance (R_s) and a polarization resistance (R_p), which is in parallel connection with the constant phase element (CPE). The fitting results are tabulated in Table 2. As far as modeling of corrosion systems is concerned, it

is important to note that the constant phase elements (CPE) is used in place of a pure double-layer capacitor. The impedance of a CPE is expressed as[21]:

$$Z_{CPE} = \frac{1}{Q(j\omega)^n} \quad (16)$$

Where Q is the CPE constant and CPE exponent, n is the phase shift which can be used as a measure of surface inhomogeneity [28]; j is an imaginary number and ω is the angular frequency in rad.s^{-1} . However, the values of C_{dl} were computed from the Q and n values, using Eq. 17[29]:

$$C_{dl} = \sqrt[n]{Q \times R_p^{1-n}} \quad (17)$$

The corrosion inhibition efficiency of studied inhibitors using EIS data can be calculated from the R_p values using the Eq. 18[21]:

$$\eta_{EIS}(\%) = \left[\frac{R_p^i - R_p^o}{R_p^i} \right] \times 100 \quad (18)$$

Where R_p^o and R_p^i are the polarization resistance in absence and presence of inhibitors respectively. Also C_{dl} and R_p are counted and presented in Table 2.

It is clearly seen from Table 2 that the polarization resistance exhibits an increasing trend with increasing benzonitrile derivatives concentration and the R_p values in inhibited solution are greater than that of uninhibited solution reached a maximum value of $382.5 \Omega \text{ cm}^2$ at $5 \times 10^{-3} \text{ M}$ in the case of PANB inhibitor. The increase in R_p values implied that a protective layer was formed on the mild steel surface, thereby retarding the charge transfer[30]. On the Other hand, adsorbed inhibitor molecules at the mild steel/electrolyte interface replace the surface adsorbed water molecules which increase the thickness of the double layer, thus leading to the reduction of C_{dl} values and therefore efficiently minimized dissolution of steel[31]. The n parameter is a measure of surface inhomogeneity. The values of n obtained from this study ranged from 0.78 to 0.84 and it is observed to decrease in the presence of the inhibitors when compared to that obtained in pure 1 M HCl, suggesting an increase in heterogeneity as a result of the adsorption of the inhibitors on the electrode/ electrolyte interface. Also, it can be seen from Table 2 that the inhibition efficiency values can be ranked as follows: PANB > APAB. Therefore, we conclude that the variation in inhibition efficiency is related to the nature of the substituent attached to the inhibitor molecules. The reason for this difference in inhibition efficiency of these compounds is better explained by DFT method and MD simulation (see theoretical section).

3.3. Weight loss study

3.3.1. Effect of concentration

By using weight loss method, the inhibition performance of organic inhibitors in studied interface can be evaluated to further confirm the electrochemical techniques results. This method is especially helpful because of its simple application and reliability. The inhibition efficiency ($\eta_{WL}(\%)$) of inhibitors, corrosion rate (C_{RW}) for mild steel specimen and the surface coverage (θ) by inhibitors obtained from weight loss experiments at different concentrations of inhibitors in 1 M HCl solution at 303K are reported in Table 3. From the results listed in Table 3, it can be observed that the corrosion rate decreases significantly with the increasing of inhibitor concentration. The rate of corrosion in the absence of inhibitors is 130.4 mm/y. While in the presence of 5×10^{-3} M of PANB and APAB, the corrosion rate reduces to 5.202 and 12.818 mm/y respectively. Decreasing of corrosion rate is due to the formation of the layer on the metal surface which covers the surface metal. It is also obvious from the Table 3 that the inhibition efficiency values for the two tested compounds attain 96.01% and 90.17% for PANB and APAB, respectively. Thus, we deduce that PANB performance is considerably better than the other inhibitor. Hence, this enhanced efficiency comes out from the adsorption of PANB molecule on mild steel surface. In short, the presence of several heteroatoms in both compounds facilitates their adsorption onto the metal surface and form a protective layer and henceforth preventing the corrosion.

3.3.2. Effect of the temperature and kinetic parameters

The effect of the temperature can provide further information on the metal-inhibitor interactions which is useful to understand the inhibition mechanism. Table 4 represents the temperature effect on the inhibition efficiency in absence and presence of 5×10^{-3} M of APAB and all concentrations of PANB. It is obvious, from this Table that the corrosion rate increased with the increasing of the temperature which suggests that a protective film of inhibitor was formed on the mild steel surface and was desorbed at a higher temperature. Arrhenius plots and transition state plots for mild steel in 1 M HCl with 5×10^{-3} M of inhibitors were represented in Figure 5 while the activation parameters derived from the slopes and intercepts of fitted lines

were summarized in Table 5. The Arrhenius and transition state equations are defined as follows[32]:

$$C_{RW} = k \exp\left(\frac{-E_a}{RT}\right) \quad (19)$$

$$C_{RW} = \frac{RT}{Nh} \exp\left(\frac{\Delta S_a}{R}\right) \exp\left(\frac{-\Delta H_a}{RT}\right) \quad (20)$$

From the results in Table 5, it can be noticed that the values of activation energy, E_a in the presence of inhibitors are generally larger than that of the uninhibited solution, which indicates the increasing of the energy barrier for the corrosion reaction[33]. In addition, the increased ΔS_a values signify an increase in the degree of disorder compared with the blank. Furthermore, we note from the Table 5 that the values of E_a and ΔH_a are varied in the same way, verifying, therefore the known thermodynamic relation:

$$E_a - \Delta H_a = RT \quad (21)$$

3.4. Adsorption isotherm

It is important to study the adsorption isotherms to understand the mechanism of inhibition corrosion reactions. To determine the most relevant isothermal model of our inhibitors, we have plotted the different models of adsorption isotherm using their mathematical formulas. From all the tested models, it can be concluded that the best fit is obtained with the Langmuir isotherm with correlation coefficients close to unity. Figure 6 represents the Langmuir adsorption isotherms of APAB and PANB at 303K and 303-333K respectively. The Langmuir adsorption isotherm is given by[34]:

$$\frac{C_{inh}}{\theta} = \frac{1}{K_{ads}} + C_{inh} \quad (22)$$

Where K_{ads} is the adsorption-desorption equilibrium constant, C_{inh} is the concentration of the benzonitrile derivatives in the solution. From the intercepts of the straight lines C_{inh}/θ vs. C_{inh} , the K_{ads} values were calculated. K_{ads} is related to the standard Gibbs free energy of adsorption, ΔG_{ads}° , by using the equation (20)[35]:

$$\Delta G_{ads}^\circ = -RT \ln(K_{ads} \times 55.5) \quad (23)$$

Where, 55.5 are the molar concentration of water, R is the universal gas constant and T is the temperature (here, 303 K). The standard enthalpy change (ΔH_{ads}°), standard entropy change (

$\Delta S_{\text{ads}}^{\circ}$) of adsorption of APNB on the steel surface can be calculated by the following equation[36]:

$$\Delta G_{\text{ads}}^{\circ} = \Delta H_{\text{ads}}^{\circ} - T\Delta S_{\text{ads}}^{\circ} \quad (24)$$

Figure 7 represents the variation of the standard Gibbs free energy as a function of the temperature while the calculated thermodynamic parameters are listed in Table 6. Based on the values of the correlation coefficient ($R^2 = 0.9999$) and the slope (close to 1), we can confirm that Langmuir model shows a good description of the adsorption behavior of inhibitors. Generally, the high values of K_{ads} indicate that the adsorption of inhibitors on the metal surface is facile as well as strong. In our present study the K_{ads} values (Table 6) of two tested inhibitors follows the order: PANB > APAB which is in accordance with the order of the inhibition efficiency. Usually, inhibitors having the values of the adsorption free energy or lower near the value -20 kJ mol^{-1} act by physical adsorption mechanism, while inhibitors with values of higher adsorption energy or close to the value -40 kJ mol^{-1} act by a chemical adsorption mechanism[37,38]. In our case, the $\Delta G_{\text{ads}}^{\circ}$ values for APNB and APAB are between the threshold values for chemical and physical adsorption, signifying that both benzonitrile derivatives adsorbed on the mild steel surface through chemical and physical adsorption[39]. In addition, this adsorption on mild steel is an exothermic process due to the negative $\Delta H_{\text{ads}}^{\circ}$ values. Besides, the value of $\Delta H_{\text{ads}}^{\circ}$ for PANB is -54 kJ/mol , which is also between the threshold values for chemical adsorption (close to -100 kJ/mol) and physical adsorption (lower than -40 kJ/mol), thus, confirming the mixed adsorption type[40]. Similar results have also been reported by other authors[36]. It has been commonly accepted that simple adsorption on the surface is usually an exothermic process, which has been accompanied by a decrease in entropy[41,42]. In our case, the same result was obtained.

3.5. Surface morphological studies

The mild steel surface was analyzed by SEM after immersion in 1.0 M HCl in absence and presence of $5 \times 10^{-3} \text{ M}$ for 6h at 303K. Figure 8 shows the surface morphology by SEM for mild steel in absence and presence of $5 \times 10^{-3} \text{ M}$ of tested inhibitors. It can be seen from this figure that the sample of steel without inhibitors is badly corroded by aggressive solution and huge corrosion products and cracks can be found on substrate surface. In the presence of inhibitors, the surface roughness decreased and this can be attributed to protective effect of tested

compounds. The morphology of steel surface in the presence of inhibitors is different and smoother than that of the free acid.

Figure 9 shows the AFM micrographs of the mild steel in absence and presence of 5×10^{-3} M of tested inhibitors. As is observed from this Figure, the surface of the mild steel is more corroded with an average roughness of 1.3 μm . When adding the optimum concentration of inhibitors, the average roughness was reduced to 461.4 nm and 790.8 nm for PANB and APAB respectively. The AFM results further confirm that PANB and APAB molecules can effectively protect the mild steel from corrosion.

3.6. Quantum chemical calculations

Generally, the inhibition effect of a compound can be well associated to its adsorption via electronic interaction with the metal surface. In recent times, quantum chemical calculations can provide more information about the structural parameters of the inhibitor molecule, while the adsorption mechanism can be accounted for the chemical reactivity of the compound[43,44]. In this case, the Frontier Molecular Orbitals (FMO) theory and geometrical optimization is useful in predicting the nature as well as extent of adsorption of the inhibitor molecules on the surface/inhibitor. The calculated quantum chemical parameters such as the highest occupied molecular orbital energy (E_{HOMO}), the lowest unoccupied molecular orbital energy (E_{LUMO}), the energy gap ($\Delta E_{\text{gap}} = E_{\text{LUMO}} - E_{\text{HOMO}}$) and the number of transferred electrons (ΔN) are important and useful tools to compare the corrosion inhibition performance of molecules and also to validate the experimental findings. The calculated theoretical parameters are given in Table 7. Figure 10 presents the optimized and frontier molecular orbitals pictures of the two inhibitors studied. Upon inspection of the geometry optimized of molecules studied (Figure 10), results reveal that, the HOMO and LUMO orbitals are distributed almost over the entire molecular structure except in acetate group. Meaning firstly, the good ability of both inhibitors to donate electrons to appropriate acceptor and on the other hand their good ability to accept electrons from the metallic surface. The HOMO energy (E_{HOMO}) is a measure of a molecule's ability to give an electron to an acceptor, while the LUMO energy (E_{LUMO}) is a measure of a molecule's proclivity to receive an electron from donor species. The higher the E_{HOMO} is, the better is the tendency of electron donation by a molecule and vice versa[45]. Lower E_{LUMO} suggests a better propensity of a molecule to receive electrons and vice versa. Therefore, higher E_{HOMO} and/or lower E_{LUMO} favor(s) higher corrosion

inhibition strength[46]. In contrast to E_{LUMO} values, the values of E_{HOMO} are not in conformity with the trend of inhibition efficiency. From a theoretical point of view, the energy gap (ΔE_{gap}) is another important factor parameter to identify the chemical reactivity of an inhibitor and their capability to be an effective corrosion inhibitor [47,48]. The adsorption performance between the inhibitors and the metal surface increases when ΔE_{gap} decreases, because the energy to remove an electron from the last occupied orbital must be lower[49]. From the table 7, it is observed that the energy gap values for APAB and PANB are 4.820 eV and 3.813 eV respectively. The compound PANB has lower energy gap (ΔE) compared to APAB. This result indicates that the adsorption performance on the steel surface of PANB is greater than that of APAB. ΔN values, on the other hand, indicate the ability of the tested inhibitor to transfer its electrons to metal if $\Delta N > 0$ and vice versa if $\Delta N < 0$. According to this criterion, it is obvious from the results in Table 7 that both compounds have higher tendency to donate electrons to a metal surface. The ΔN values follow the same order of the E_{LUMO} values which signifies that the electron accepting ability of the inhibitor molecules plays the crucial role in the difference between investigated compounds[50,51].

In corrosion inhibition research, the Fukui indices are an important descriptor to explore the relationship of the inhibitors with MS surface in terms of structure-activity. This study provides an exciting opportunity to strengthen our knowledge of electron donating capacity (i.e. nucleophilic f_k^+), and electron accepting ability (i.e. electrophilic f_k^-) of inhibitors molecules. The results are summarized in Table 8 from which we notice that in the case of APAB molecule, the C (1), C(5), C(31) and N (32) atoms are the highest values of f_k^+ indicating that these atoms are available to accept electrons from the metal surface. On the other hand, the N(10), N (28) and N(32) atoms possess higher values of f_k^- which means that they are responsible for the electrophilic attack. In the case of the compound PANB, it is clear that the addition of acceptor group $-\text{NO}_2$ leads to the new distribution of the active sites. It is evidently clear from Table 8 that the C(3), N(12), O(13) and O(14) atoms are the active sites susceptible for nucleophilic attacks. However, the electrophilic sites are present in N(11) and N(15) atoms. The theoretical study shows that the introduction of the nitro group has a positive effect on the reactivity of the compound PANB which is consistent with experimental observations.

3.7. Molecular dynamics simulations

Since strong correlation exists between electronic properties of inhibitor and corrosion effectiveness, DFT calculations are very useful for the overall understanding of electronic properties of corrosion inhibitors [52]. On the other side, understanding the interactions of inhibitor molecules with the metal surface are also of great importance. In this case, MD simulations can be particularly useful for the determination of molecule's atoms with strong interaction with the metal surface, which can be useful for the understanding of corrosion inhibition process. The binding and interaction energies of the adsorbed inhibitors have been approximated when the simulation system reached its equilibrium state[53]. The best adsorption configuration of the studied molecules on Fe (110) surface is shown in Figure 11 while the interaction and binding energies are placed in Table 9. Looking at Figure 11, what stands out is that all inhibitor molecules had been moved in nearly parallel or flat disposition which provide larger blocking area by the investigated inhibitors preventing the surface from corrosion through a formation of a barrier layer between the metal surface and the aggressive media. The large negative values of the interaction energies for both inhibitors indicating that the interaction between inhibitor molecules and Fe(110) surface is spontaneous, strong and stable [12]. On the other hand, the high magnitude of the binding energies suggests that the adsorption system is more stable and that there is more than one bond to the iron surface per inhibitor molecules [54].

In order to locate the atoms of inhibitor molecule with relatively significant interactions with the metal surface, we have calculated RDFs after MD simulations [55]. According to the studies in the literature, the length of the small links is indicated by the peak which produces at $1 \text{ \AA} \sim 3.5 \text{ \AA}$, which correlated to chemisorption, while the peaks longer than 3.5 \AA prove that there is a physical interaction[22,56]. The RDFs of all non-hydrogen atoms of the two inhibitors are displayed in Figure 12. From this Figure, the radial distribution function of C, N and O atoms in the case of PANB shows that the bonding length of Fe–N (3.1 \AA), Fe–O (2.9 \AA) and Fe–C (3.3 \AA) are all less than 3.5 \AA , while for APAB, are 3.1 \AA for Fe–C and 2.34 \AA for Fe–N. This extensive research has shown the chemical interaction between inhibitor compounds and MS surface, and the highest protection of metal surface through an effective adsorption of benzonitrile compounds. As the previously mentioned in the theoretical and experimental parts, the presence of the nitro group provides good inhibitive properties. Therefore, the difference between the two tested compounds may be attributed to the electron density and the number of the reactive centers in each molecule.

4. Conclusion

The present study was designed to evaluate the corrosion inhibition activity of novel benzonitrile derivatives using weight loss, EIS, PDP measurements and theoretical calculations. The results of both gravimetric and electrochemical experiments showed that the two compounds inhibit mild steel corrosion in 1 M HCl solution and the inhibition efficiency increases with increasing concentration of the inhibitors, reaching its maximum value at 5×10^{-3} M in the case of PANB ($\approx 96.01\%$). The corrosion process is inhibited by the adsorption of PANB and APAB on steel surface and the adsorption of these inhibitors fits a Langmuir isotherm model. Based on the PDP results, PANB and APAB can be classified as mixed inhibitors. The polarization resistance of these two inhibitors is highest with 5×10^{-3} M when compared to the value obtained for the blank solution. The quantum chemical by DFT calculations and molecular dynamics simulations give a better overview of the reactivity of tested inhibitors towards mild steel. The results indicate that PANB had a stronger interaction with the steel than APAB, which corroborate with experimental results. These outcomes are important towards rational design of new corrosion inhibitors.

ACKNOWLEDGEMENTS

The authors extend their appreciation to the Deanship of Scientific Research at King Khalid University for funding this work through research groups program under grant number R.G.P-1.21-38.

REFERENCES

- [1] N.A. Negm, M.A. El Hashash, A. Abd-Elaal, S.M. Tawfik, A. Gharieb, Amide type nonionic surfactants: Synthesis and corrosion inhibition evaluation against carbon steel corrosion in acidic medium, *J. Mol. Liq.* (2018). doi:10.1016/j.molliq.2018.02.078.
- [2] L. Jiang, Y. Qiang, Z. Lei, J. Wang, Z. Qin, B. Xiang, Excellent corrosion inhibition performance of novel quinoline derivatives on mild steel in HCl media: Experimental and computational investigations, *J. Mol. Liq.* 255 (2018) 53–63. doi:10.1016/j.molliq.2018.01.133.
- [3] C. Verma, L.O. Olasunkanmi, E.E. Ebenso, M.A. Quraishi, Substituents effect on corrosion inhibition performance of organic compounds in aggressive ionic solutions: A review, *J. Mol. Liq.* 251 (2018) 100–118. doi:10.1016/j.molliq.2017.12.055.
- [4] M.A. Bedair, The effect of structure parameters on the corrosion inhibition effect of some heterocyclic nitrogen organic compounds, *J. Mol. Liq.* 219 (2016) 128–141. doi:10.1016/j.molliq.2016.03.012.

- [5] G.H. Sayed, M.E. Azab, K.E. Anwer, M.A. Raouf, N.A. Negm, Pyrazole, pyrazolone and enamionitrile pyrazole derivatives: Synthesis, characterization and potential in corrosion inhibition and antimicrobial applications, *J. Mol. Liq.* 252 (2018) 329–338. doi:10.1016/j.molliq.2017.12.156.
- [6] A. Fouda, R. Fouad, New azonitrile derivatives as corrosion inhibitors for copper in nitric acid solution, *Cogent Chem.* 2 (2016) 1221174.
- [7] R. Agrawal, T. Namboodhiri, Inhibition of corrosion and hydrogen embrittlement of a HSLA steel in 0.5 M H₂SO₄ by nitrile compounds, *J. Appl. Electrochem.* 27 (1997) 1265–1274.
- [8] A. Fouda, M. Diab, S. Fathy, Role of Some Organic Compounds as Corrosion Inhibitors for 316L Stainless Steel in 1 M HCl, *Int. J. Electrochem. Sci.* 12 (2017) 347–362.
- [9] Z. Salarvand, M. Amirnasr, M. Talebian, K. Raeissi, S. Meghdadi, Enhanced corrosion resistance of mild steel in 1 M HCl solution by trace amount of 2-phenyl-benzothiazole derivatives: Experimental, quantum chemical calculations and molecular dynamics (MD) simulation studies, *Corros. Sci.* 114 (2017) 133–145.
- [10] R. Wu, X. Qiu, Y. Shi, M. Deng, Molecular dynamics simulation of the atomistic monolayer structures of N-acyl amino acid-based surfactants, *Mol. Simul.* 43 (2017) 491–501.
- [11] M. Hegazy, A. Badawi, S.A. El Rehim, W. Kamel, Corrosion inhibition of carbon steel using novel N-(2-(2-mercaptoacetoxy) ethyl)-N, N-dimethyl dodecan-1-aminium bromide during acid pickling, *Corros. Sci.* 69 (2013) 110–122.
- [12] C. Verma, M. Quraishi, A. Singh, 2-Amino-5-nitro-4, 6-diarylcyclohex-1-ene-1, 3, 3-tricarbonitriles as new and effective corrosion inhibitors for mild steel in 1 M HCl: Experimental and theoretical studies, *J. Mol. Liq.* 212 (2015) 804–812.
- [13] D.K. Singh, S. Kumar, G. Udayabhanu, R.P. John, 4 (N, N-dimethylamino) benzaldehyde nicotinic hydrazone as corrosion inhibitor for mild steel in 1 M HCl solution: An experimental and theoretical study, *J. Mol. Liq.* 216 (2016) 738–746.
- [14] Z. Zhang, N. Tian, X. Huang, W. Shang, L. Wu, Synergistic inhibition of carbon steel corrosion in 0.5 M HCl solution by indigo carmine and some cationic organic compounds: experimental and theoretical studies, *RSC Adv.* 6 (2016) 22250–22268.
- [15] R.G. Pearson, Hard and soft acids and bases—the evolution of a chemical concept, *Coord. Chem. Rev.* 100 (1990) 403–425.
- [16] Z. Cao, Y. Tang, H. Cang, J. Xu, G. Lu, W. Jing, Novel benzimidazole derivatives as corrosion inhibitors of mild steel in the acidic media. Part II: Theoretical studies, *Corros. Sci.* 83 (2014) 292–298.
- [17] I. Obot, D. Macdonald, Z. Gasem, Density functional theory (DFT) as a powerful tool for designing new organic corrosion inhibitors. Part 1: an overview, *Corros. Sci.* 99 (2015) 1–30.
- [18] A. Dutta, S.K. Saha, P. Banerjee, A.K. Patra, D. Sukul, Evaluating corrosion inhibition property of some Schiff bases for mild steel in 1 M HCl: competitive effect of the heteroatom and stereochemical conformation of the molecule, *RSC Adv.* 6 (2016) 74833–74844.
- [19] M. Bouanis, M. Tourabi, A. Nyassi, A. Zarrouk, C. Jama, F. Bentiss, Corrosion inhibition performance of 2, 5-bis (4-dimethylaminophenyl)-1, 3, 4-oxadiazole for carbon steel in HCl solution: Gravimetric, electrochemical and XPS studies, *Appl. Surf. Sci.* 389 (2016) 952–966.
- [20] D. Zhang, Y. Tang, S. Qi, D. Dong, H. Cang, G. Lu, The inhibition performance of long-chain alkyl-substituted benzimidazole derivatives for corrosion of mild steel in HCl, *Corros. Sci.* 102 (2016) 517–522.

- [21] H. Lgaz, R. Salghi, S. Jodeh, B. Hammouti, Effect of clozapine on inhibition of mild steel corrosion in 1.0 M HCl medium, *J. Mol. Liq.* 225 (2017) 271–280.
- [22] S.-W. Xie, Z. Liu, G.-C. Han, W. Li, J. Liu, Z. Chen, Molecular dynamics simulation of inhibition mechanism of 3, 5-dibromo salicylaldehyde Schiff's base, *Comput. Theor. Chem.* 1063 (2015) 50–62.
- [23] F. Bentiss, F. Gassama, D. Barbry, L. Gengembre, H. Vezin, M. Lagrenée, M. Traisnel, Enhanced corrosion resistance of mild steel in molar hydrochloric acid solution by 1,4-bis(2-pyridyl)-5H-pyridazino[4,5-b]indole: Electrochemical, theoretical and XPS studies, *Appl. Surf. Sci.* 252 (2006) 2684–2691. doi:10.1016/j.apsusc.2005.03.231.
- [24] H. Lgaz, K. Subrahmanya Bhat, R. Salghi, Shubhalaxmi, S. Jodeh, M. Algarra, B. Hammouti, I.H. Ali, A. Essamri, Insights into corrosion inhibition behavior of three chalcone derivatives for mild steel in hydrochloric acid solution, *J. Mol. Liq.* 238 (2017) 71–83. doi:10.1016/j.molliq.2017.04.124.
- [25] C. Verma, M. Quraishi, A. Singh, 2-Amino-5-nitro-4, 6-diarylcyclohex-1-ene-1, 3, 3-tricarbonitriles as new and effective corrosion inhibitors for mild steel in 1M HCl: Experimental and theoretical studies, *J. Mol. Liq.* 212 (2015) 804–812.
- [26] D.K. Singh, S. Kumar, G. Udayabhanu, R.P. John, 4 (N, N-dimethylamino) benzaldehyde nicotinic hydrazone as corrosion inhibitor for mild steel in 1M HCl solution: An experimental and theoretical study, *J. Mol. Liq.* 216 (2016) 738–746.
- [27] D. Zhang, Y. Tang, S. Qi, D. Dong, H. Cang, G. Lu, The inhibition performance of long-chain alkyl-substituted benzimidazole derivatives for corrosion of mild steel in HCl, *Corros. Sci.* 102 (2016) 517–522.
- [28] W. Chen, S. Hong, B. Xiang, H. Luo, M. Li, N. Li, Corrosion inhibition of copper in hydrochloric acid by coverage with trithiocyanuric acid self-assembled monolayers, *Corros. Eng. Sci. Technol.* 48 (2013) 98–107.
- [29] S. Martinez, M. Metikoš-Huković, A nonlinear kinetic model introduced for the corrosion inhibitive properties of some organic inhibitors, *J. Appl. Electrochem.* 33 (2003) 1137–1142.
- [30] S.K. Saha, A. Dutta, P. Ghosh, D. Sukul, P. Banerjee, Novel Schiff-base molecules as efficient corrosion inhibitors for mild steel surface in 1 M HCl medium: experimental and theoretical approach, *Phys. Chem. Chem. Phys.* 18 (2016) 17898–17911.
- [31] A. Ongun Yüce, B. Doğru Mert, G. Kardaş, B. Yazıcı, Electrochemical and quantum chemical studies of 2-amino-4-methyl-thiazole as corrosion inhibitor for mild steel in HCl solution, *Corros. Sci.* 83 (2014) 310–316. doi:10.1016/j.corsci.2014.02.029.
- [32] M. Larouj, H. Lgaz, R. Salghi, H. Serrar, S. Boukhris, S. Jodeh, Experimental and quantum chemical analysis of new pyrimidothiazine derivative as corrosion inhibitor for mild steel in 1.0 M hydrochloric acid solution, *Anal. Bioanal. Electrochem.* 10 (2018) 33–51.
- [33] C. Verma, L.O. Olasunkanmi, E.E. Ebenso, M.A. Quraishi, I.B. Obot, Adsorption Behavior of Glucosamine-Based, Pyrimidine-Fused Heterocycles as Green Corrosion Inhibitors for Mild Steel: Experimental and Theoretical Studies, *J. Phys. Chem. C.* 120 (2016) 11598–11611. doi:10.1021/acs.jpcc.6b04429.
- [34] S. Garai, S. Garai, P. Jaisankar, J. Singh, A. Elango, A comprehensive study on crude methanolic extract of *Artemisia pallens* (Asteraceae) and its active component as effective corrosion inhibitors of mild steel in acid solution, *Corros. Sci.* 60 (2012) 193–204.
- [35] M.S. Morad, Inhibition of iron corrosion in acid solutions by Cefatrexyl: Behaviour near and at the corrosion potential, *Corros. Sci.* 50 (2008) 436–448.
- [36] M. Yadav, R.R. Sinha, T.K. Sarkar, N. Tiwari, Corrosion inhibition effect of pyrazole derivatives on mild steel in hydrochloric acid solution, *J. Adhes. Sci. Technol.* 29 (2015) 1690–1713.

- [37] A.K. Singh, M.A. Quraishi, Investigation of the effect of disulfiram on corrosion of mild steel in hydrochloric acid solution, *Corros. Sci.* 53 (2011) 1288–1297.
- [38] M.J. Bahrami, S.M.A. Hosseini, P. Pilvar, Experimental and theoretical investigation of organic compounds as inhibitors for mild steel corrosion in sulfuric acid medium, *Corros. Sci.* 52 (2010) 2793–2803.
- [39] H. Ma, S. Chen, Z. Liu, Y. Sun, Theoretical elucidation on the inhibition mechanism of pyridine–pyrazole compound: A Hartree Fock study, *J. Mol. Struct. THEOCHEM.* 774 (2006) 19–22.
- [40] S. Martinez, I. Stern, Thermodynamic characterization of metal dissolution and inhibitor adsorption processes in the low carbon steel/mimosa tannin/sulfuric acid system, *Appl. Surf. Sci.* 199 (2002) 83–89.
- [41] B. Ateya, B. El-Anadouli, F. El-Nizamy, The adsorption of thiourea on mild steel, *Corros. Sci.* 24 (1984) 509–515.
- [42] J.M. Thomas, W.J. Thomas, Principles and practice of heterogeneous catalysis, John Wiley & Sons, 2014.
- [43] M. Yadav, D. Behera, S. Kumar, Experimental and theoretical investigation on adsorption and corrosion inhibition properties of imidazopyridine derivatives on mild steel in hydrochloric acid solution, *Surf. Interface Anal.* 46 (2014) 640–652.
- [44] B. Gómez, N. Likhanova, M. Dominguez Aguilar, O. Olivares, J. Hallen, J. Martínez-Magadán, Theoretical study of a new group of corrosion inhibitors, *J. Phys. Chem. A.* 109 (2005) 8950–8957.
- [45] I. Danaee, O. Ghasemi, G. Rashed, M.R. Awei, M. Maddahy, Effect of hydroxyl group position on adsorption behavior and corrosion inhibition of hydroxybenzaldehyde Schiff bases: Electrochemical and quantum calculations, *J. Mol. Struct.* 1035 (2013) 247–259.
- [46] F. El-Hajjaji, M. Messali, A. Aljuhani, M. Aouad, B. Hammouti, M. Belghiti, D. Chauhan, M. Quraishi, Pyridazinium-based ionic liquids as novel and green corrosion inhibitors of carbon steel in acid medium: Electrochemical and molecular dynamics simulation studies, *J. Mol. Liq.* 249 (2018) 997–1008.
- [47] M. Yadav, D. Behera, S. Kumar, Experimental and theoretical investigation on adsorption and corrosion inhibition properties of imidazopyridine derivatives on mild steel in hydrochloric acid solution, *Surf. Interface Anal.* 46 (2014) 640–652.
- [48] B. Gómez, N.V. Likhanova, M.A. Dominguez Aguilar, O. Olivares, J.M. Hallen, J.M. Martínez-Magadán, Theoretical study of a new group of corrosion inhibitors, *J. Phys. Chem. A.* 109 (2005) 8950–8957.
- [49] S. Deng, X. Li, X. Xie, Hydroxymethyl urea and 1, 3-bis (hydroxymethyl) urea as corrosion inhibitors for steel in HCl solution, *Corros. Sci.* 80 (2014) 276–289.
- [50] N. Kovačević, A. Kokalj, Analysis of molecular electronic structure of imidazole-and benzimidazole-based inhibitors: a simple recipe for qualitative estimation of chemical hardness, *Corros. Sci.* 53 (2011) 909–921.
- [51] A. Kokalj, Is the analysis of molecular electronic structure of corrosion inhibitors sufficient to predict the trend of their inhibition performance, *Electrochimica Acta.* 56 (2010) 745–755.
- [52] F.E. Awe, S.O. Idris, M. Abdulwahab, E.E. Oguzie, Theoretical and experimental inhibitive properties of mild steel in HCl by ethanolic extract of *Boscia senegalensis*, *Cogent Chem.* 1 (2015) 1112676.
- [53] H. Lgaz, R. Salghi, S. Jodeh, B. Hammouti, Effect of clozapine on inhibition of mild steel corrosion in 1.0 M HCl medium, *J. Mol. Liq.* 225 (2017) 271–280.
- [54] A. Kokalj, Comments on the “Reply to comments on the paper ‘On the nature of inhibition performance of imidazole on iron surface’” by JO Mendes and AB Rocha, *Corros. Sci.* 70 (2013) 294–297.

- [55] S.-W. Xie, Z. Liu, G.-C. Han, W. Li, J. Liu, Z. Chen, Molecular dynamics simulation of inhibition mechanism of 3, 5-dibromo salicylaldehyde Schiff's base, *Comput. Theor. Chem.* 1063 (2015) 50–62.
- [56] Z. Zhang, N. Tian, X. Huang, W. Shang, L. Wu, Synergistic inhibition of carbon steel corrosion in 0.5 M HCl solution by indigo carmine and some cationic organic compounds: experimental and theoretical studies, *RSC Adv.* 6 (2016) 22250–22268.

ACCEPTED MANUSCRIPT

Figures captions:

Fig. 1: Schematic representation of the benzonitrile derivatives.

Fig. 2: Potentiodynamic polarization curves of mild steel in 1 M HCl at various concentrations of PANB and APAB at 303K.

Fig. 3: Nyquist diagrams of mild steel in 1 M HCl in the absence and presence of different concentrations of: (a) PANB and (b) APAB at 303K.

Fig. 4: Equivalent circuit employed to fitting and simulation of the impedance spectra.

Fig. 5: Arrhenius and transition state plots for corrosion inhibition of mild steel in absence and presence of 5×10^{-3} M of inhibitor in 1.0 M HCl

Fig. 6: Plots of the Langmuir adsorption isotherm on mild steel in 1 M HCl containing various concentrations of PANB and APAB at different temperatures.

Fig. 7. The variation of the standard Gibbs free energy as a function of the temperature.

Fig. 8: SEM images of MS: (a) exposed to 1 M HCl, (b) and (c) exposed to 1.0 M HCl + 5×10^{-3} M of PANB and APAB respectively, after 6 h of immersion time at 303 K.

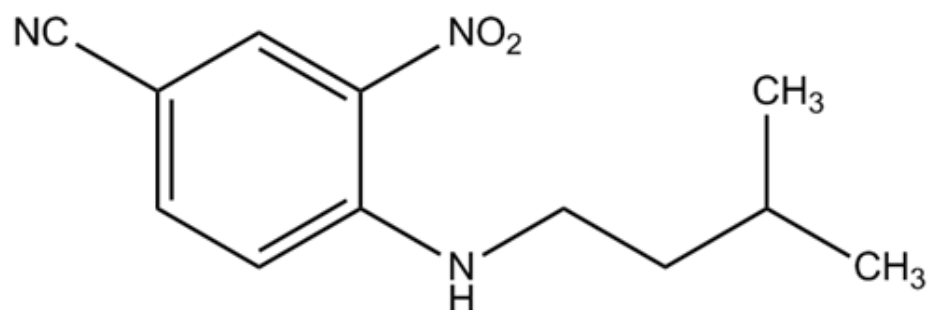
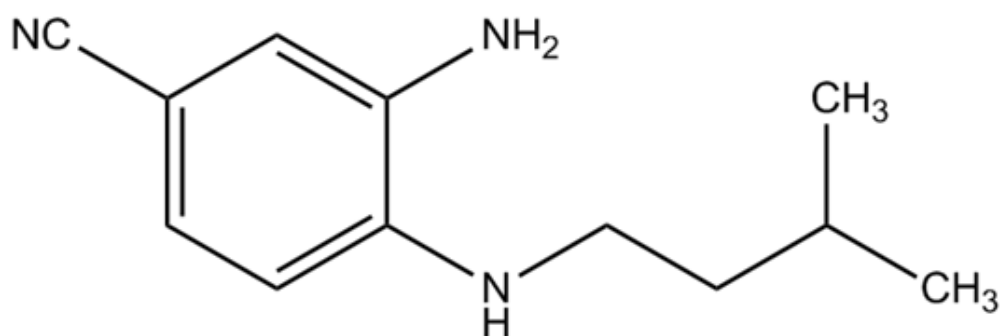
Fig. 9: AFM images of MS surface in absence and presence of tested inhibitors at 5×10^{-3} M of inhibitors after 6 h of immersion time at 303 K.

Fig. 10: (A) The optimized geometry, (B) HOMO and (C) LUMO of the inhibitors molecules. [atom legend: white=H; Gray=C; blue=N; red = O].

Fig. 11: Top and side views of the final adsorption of the benzonitrile derivatives on the Fe (110) surface in solution.

Fig. 12: RDFs analysis of C, N, and O atoms from APAB and PANB adsorbed on the Fe (110) surface.

Fig. 1

4-(isopentylamino)-3-nitrobenzonitrile (**PANB**)3-amino-4-(isopentylamino)benzonitrile (**APAB**)

AC

Fig. 2

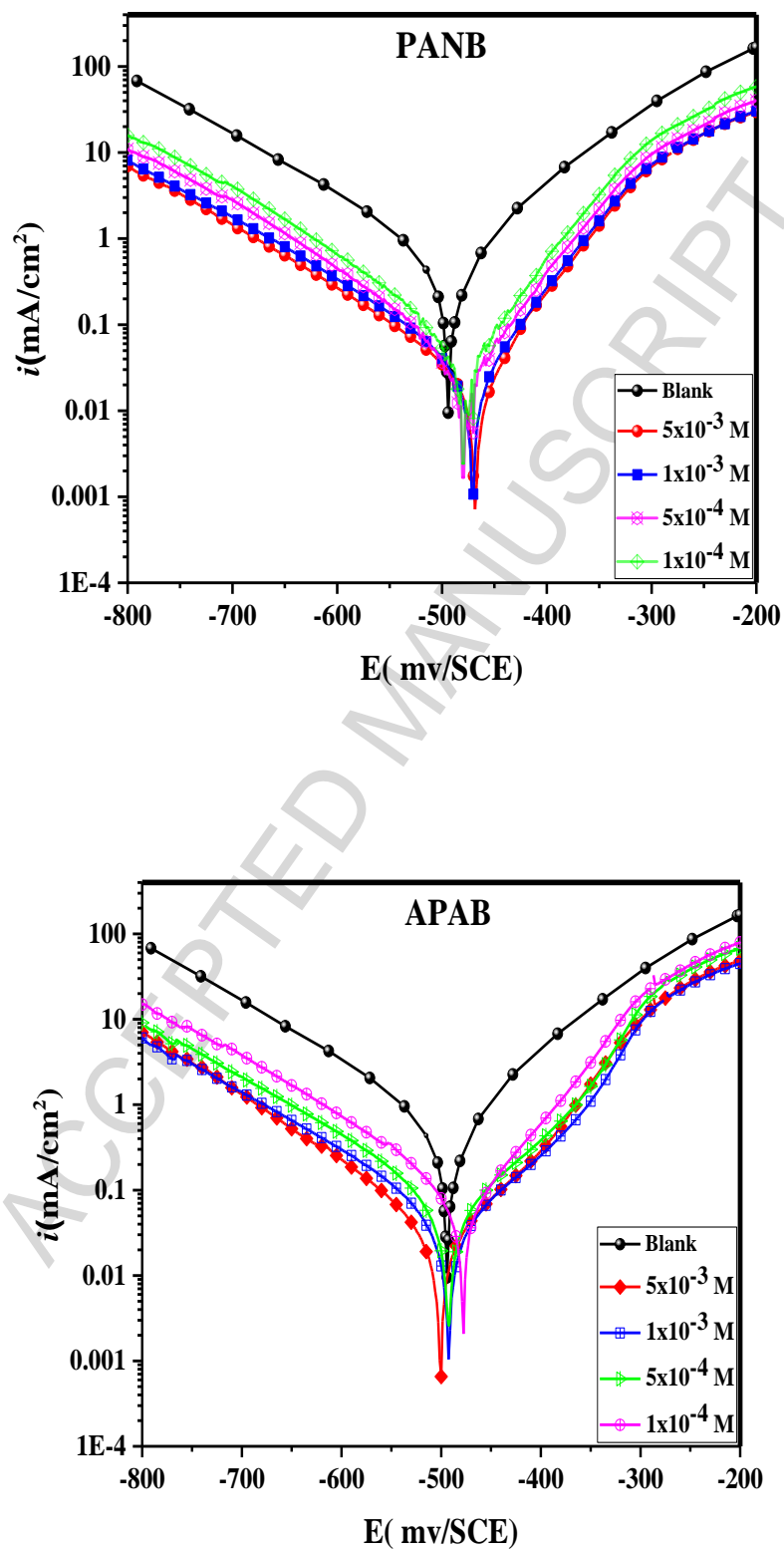


Fig. 3

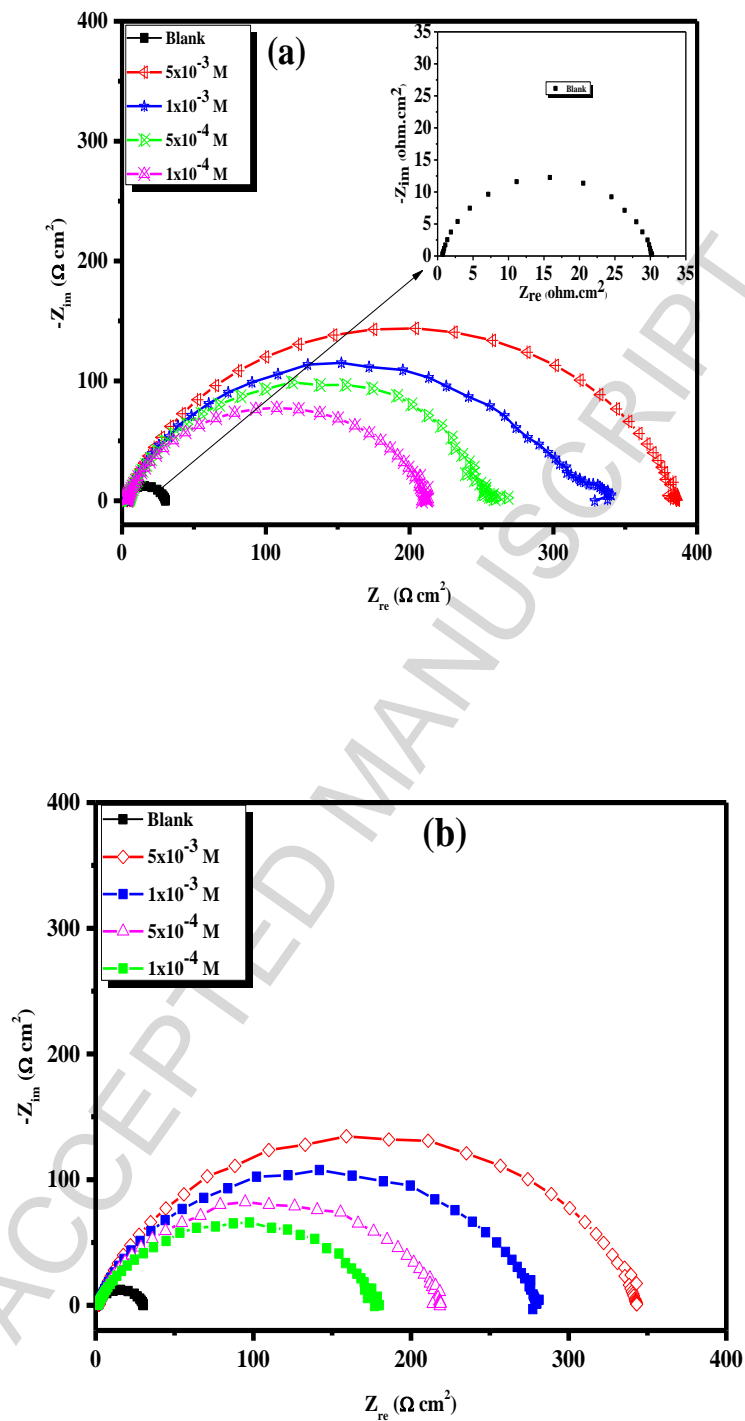
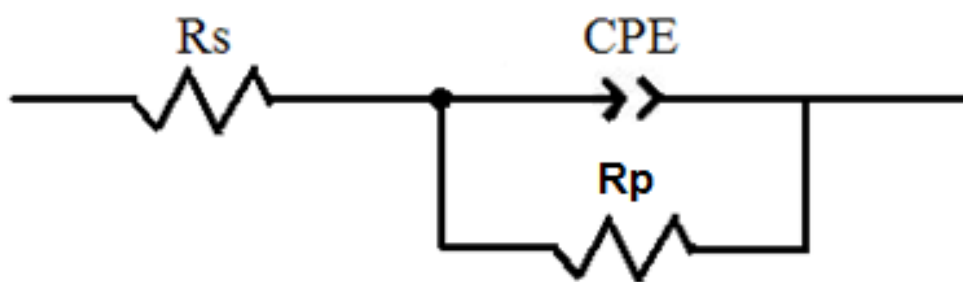


Fig. 4



ACCEPTED MANUSCRIPT

Fig. 5

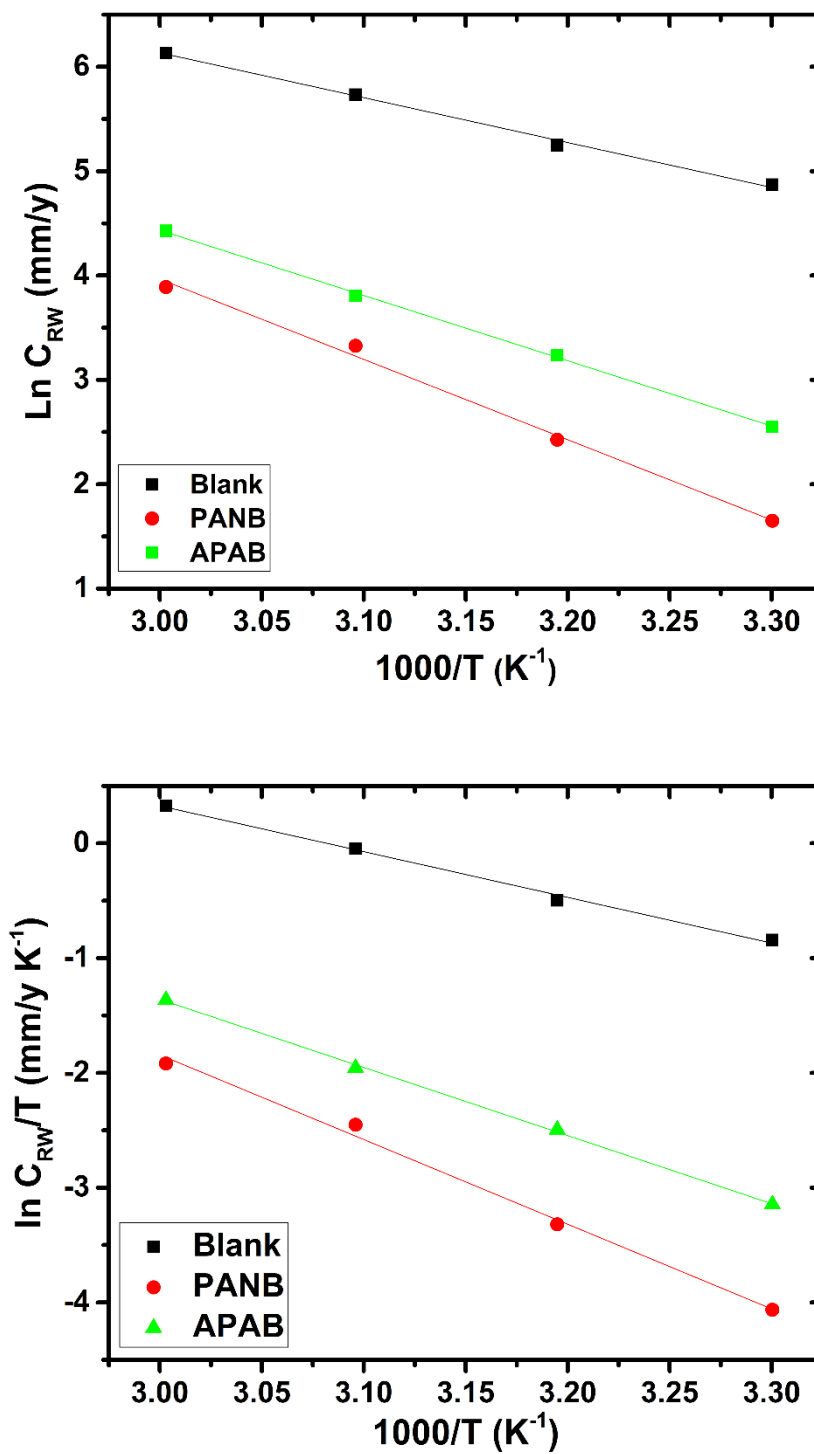


Fig. 6

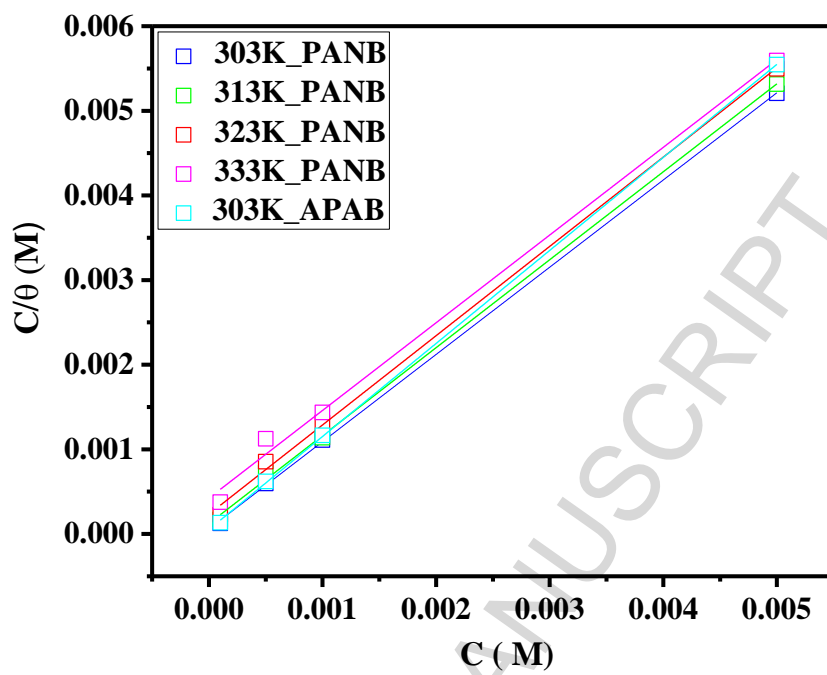


Fig. 7

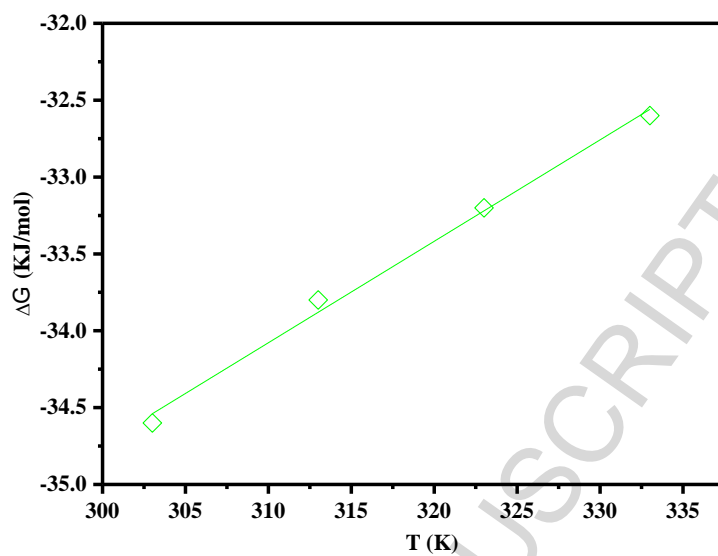


Fig. 8

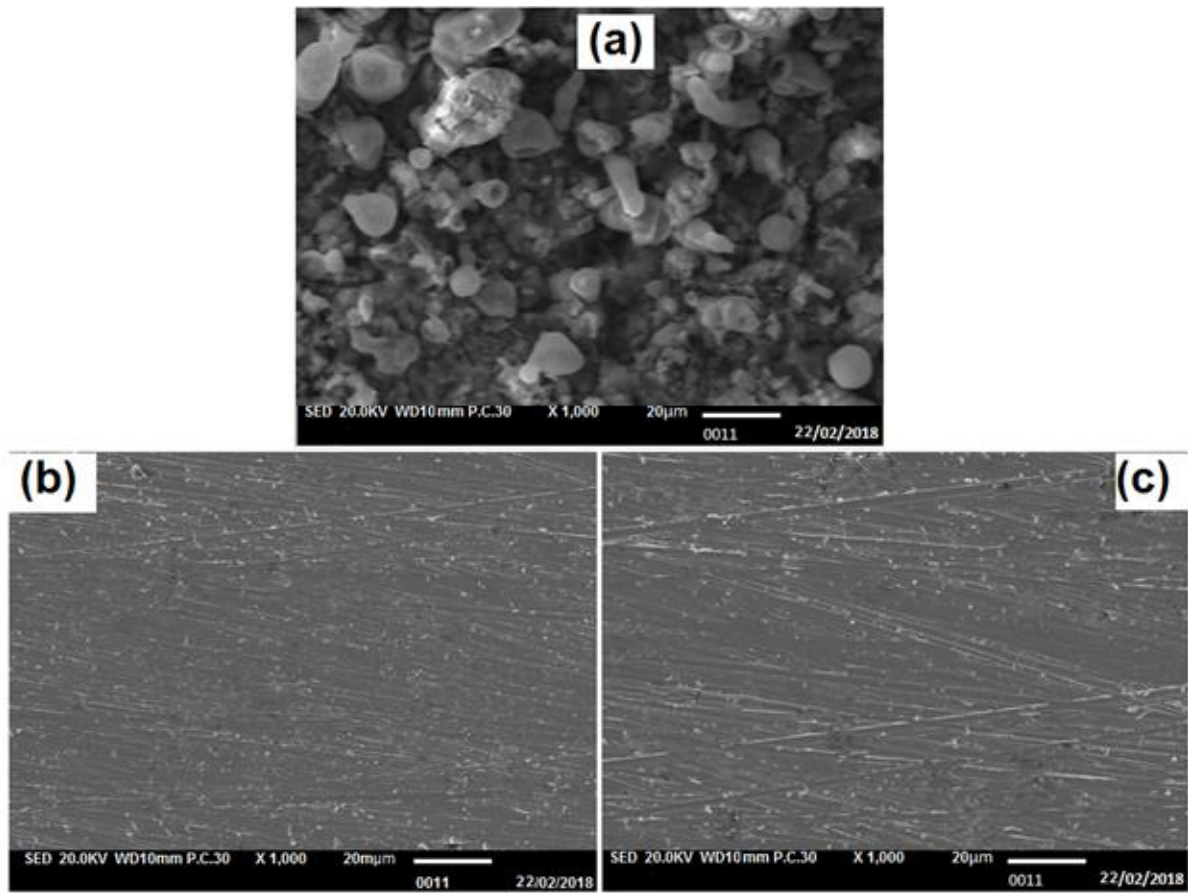


Fig. 9

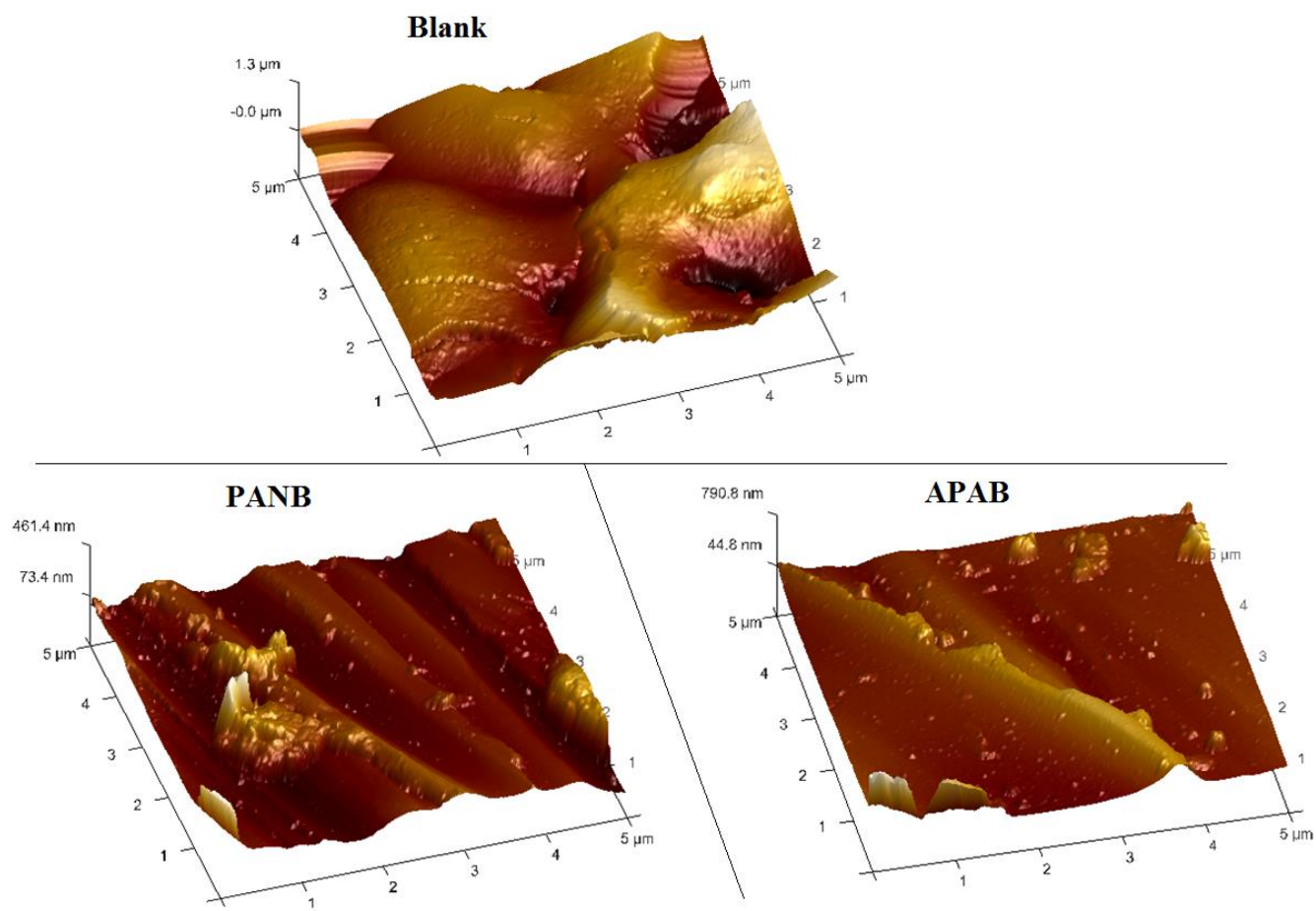


Fig. 10

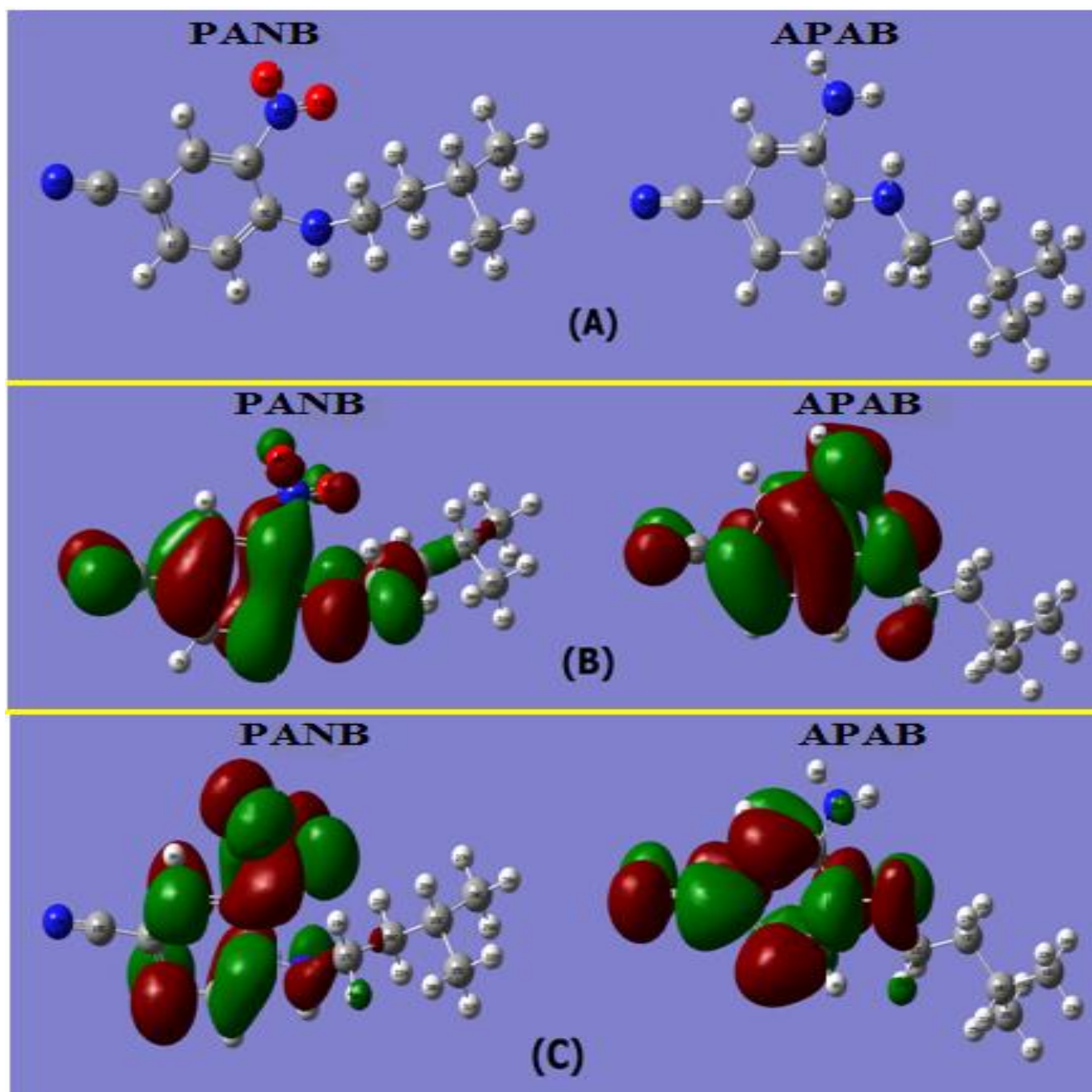


Fig. 11

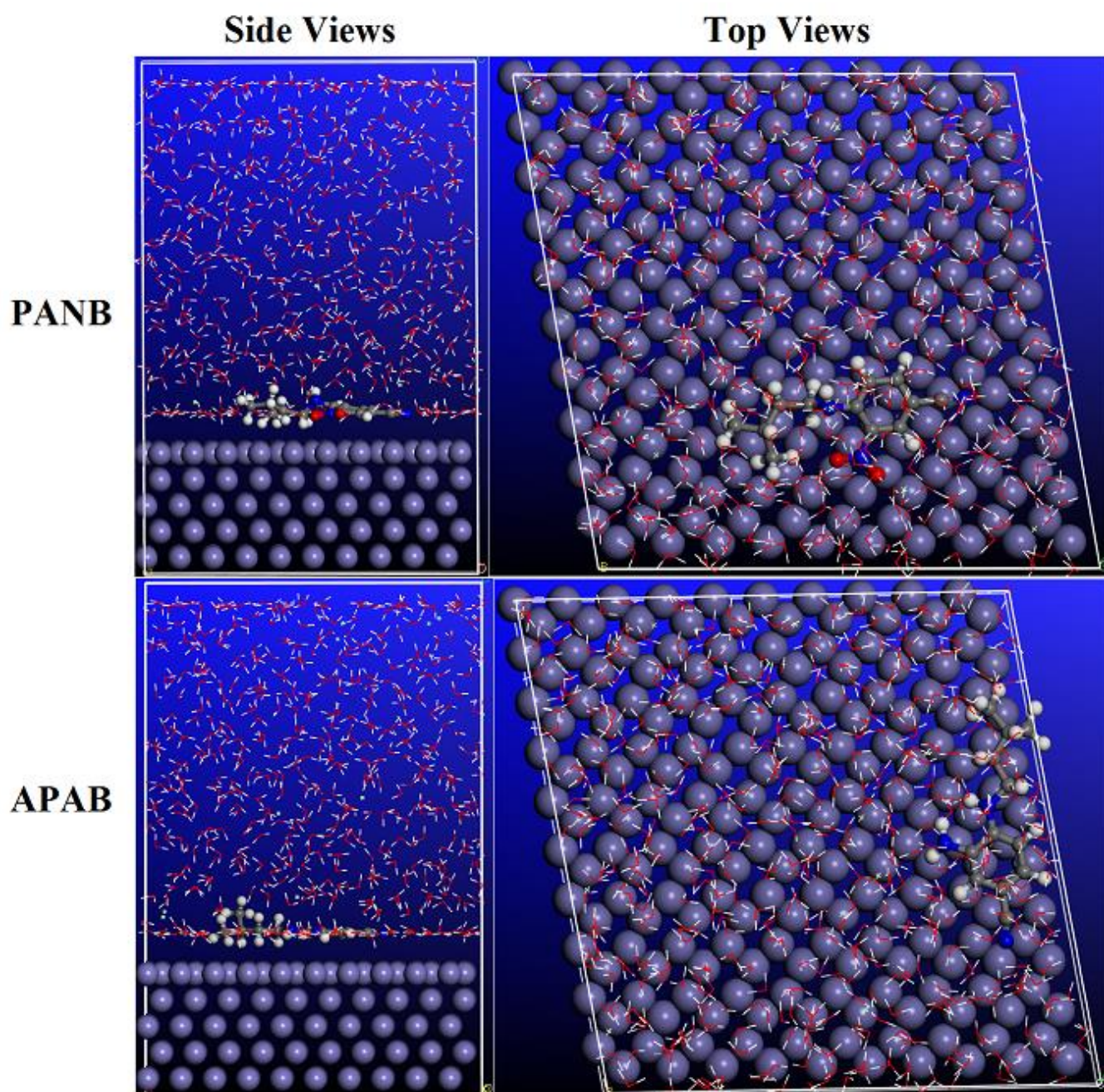
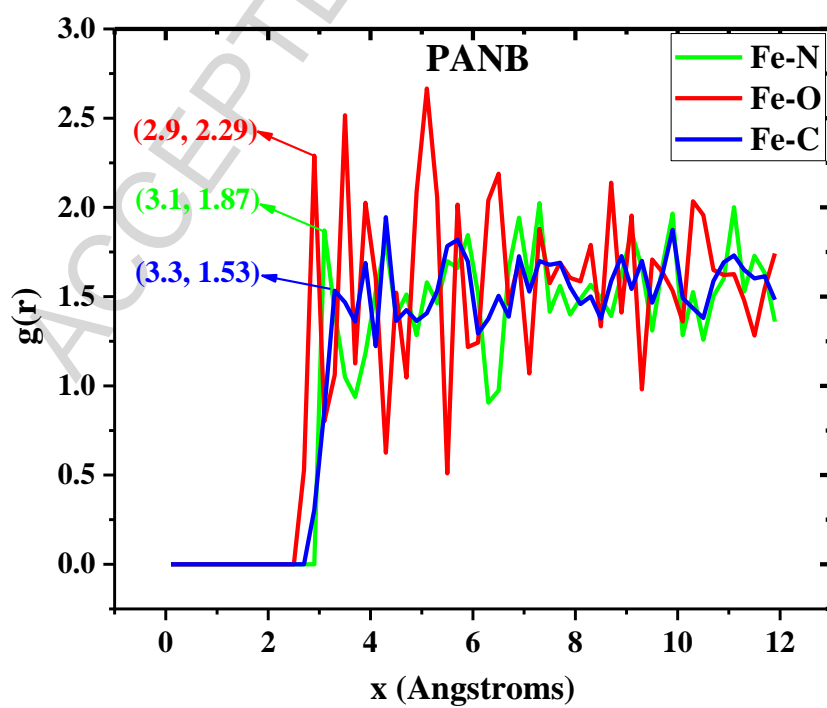
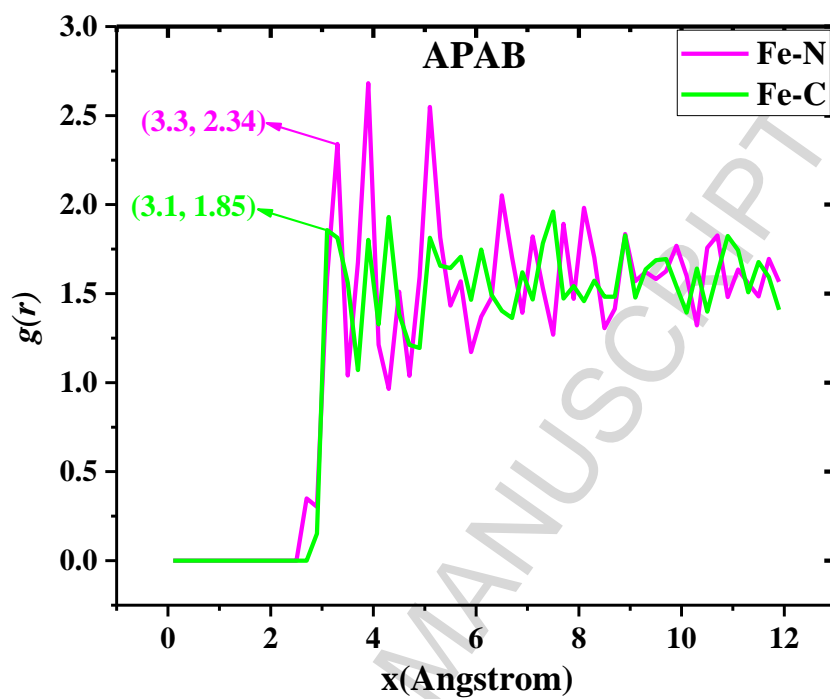


Fig. 12



Tables:**Table 1.** Electrochemical parameter values evaluated from potentiodynamic polarization curves for mild steel in 1 M HCl at various inhibitors concentrations at 303K.

Inhibitors	Concentration (M)	$-E_{corr}$ (mV/SCE)	$-\beta_c$ (mV dec ⁻¹)	β_a (mV/dec)	i_{corr} ($\mu\text{A cm}^{-2}$)	η_{PDP} (%)	Θ
HCl	1.0	496	162	132.2	564	-	-
	5×10^{-3}	470.6	129.5	67.3	25.8	95.42	0.95
PANB	1×10^{-3}	473.4	130.6	71.7	34.9	93.81	0.93
	5×10^{-4}	480.2	126.7	76.6	50.9	90.97	0.90
	1×10^{-4}	480.7	154.5	89.8	71.5	87.32	0.87
APAB	5×10^{-3}	503.4	125.4	82.1	34.6	93.86	0.93
	1×10^{-3}	495.2	148.0	87.4	56.2	90.03	0.90
	5×10^{-4}	495	147.5	77.6	84.2	85.07	0.85
	1×10^{-4}	473	153.0	71.7	93.3	83.45	0.83

Table 2. EIS parameters for mild steel in the acid medium at various concentrations of PANB and APAB at 303K.

Inhibitors	Concentration (M)	R_p ($\Omega \times \text{cm}^2$)	n	$Q \times 10^{-4}$ ($\text{s}^n / \Omega \times \text{cm}^2$)	C_{dl} ($\mu\text{F}/\text{cm}^2$)	η_{EIS} (%)
HCl	1.0	29.35	0.89	1.7610	91	-
	5×10^{-3}	382.5	0.78	0.3850	11	92.32
PANB	1×10^{-3}	322.1	0.79	0.3919	12	90.88
	5×10^{-4}	262.1	0.81	0.4297	14	88.75
	1×10^{-4}	208.9	0.80	0.5372	17	85.95
APAB	5×10^{-3}	341.5	0.84	0.3805	16	91.40
	1×10^{-3}	278.8	0.79	0.6728	23	89.47
	5×10^{-4}	218.4	0.81	0.6433	25	86.56
	1×10^{-4}	177.9	0.78	0.9265	29	83.50

Table 3. Corrosion rate and inhibition efficiency of mild steel in 1 M HCl immersed in various concentrations of inhibitors obtained by weight loss method at 303 K.

Inhibitors	Concentration (M)	C_{RW} (mm/y)	η_{WL} (%)	Θ
HCl	1.0	130.4	-	-
	5×10^{-3}	5.202	96.01	0.96
PANB	1×10^{-3}	13.00	90.03	0.90
	5×10^{-4}	21.229	83.72	0.82
	1×10^{-4}	26.979	79.31	0.79
APAB	5×10^{-3}	12.818	90.17	0.90
	1×10^{-3}	18.503	85.81	0.85
	5×10^{-4}	25.401	80.52	0.80
	1×10^{-4}	32.821	74.83	0.74

Table 4. Corrosion rate and inhibition efficiency of mild steel in 1 M HCl in absence and in presence of inhibitors at different temperatures

Inhibitors	Concentration (M)	303K		313K		323K		333K	
		C_{RW} (mm/y)	η_{WL} (%)						
Blank	1	130.4	-	190.2	-	308.6	-	460.4	-
APAB	5×10^{-3}	12.818	90	25.432	86	44.911	85	83.801	81
	5×10^{-3}	5.202	96	11.321	94	27.805	91	48.863	89
PANB	1×10^{-3}	13.000	90	23.018	87	73.973	76	139.842	69
	5×10^{-4}	21.229	83	58.983	69	128.068	58	255.822	44
	1×10^{-4}	26.979	79	78.871	58	174.104	43	338.087	26

Table 5. Corrosion kinetic parameters for mild steel in 1.0 M HCl in the presence and absence of 5×10^{-3} M of inhibitors.

Inhibitors	E_a (kJ/mol)	ΔH_a (kJ/mol)	ΔS_a (J mol⁻¹ K⁻¹)	$E_a - \Delta H_a$
Blank	35.77	33.13	-95.36	2.64
PANB	63.98	61.34	-28.76	2.64
APAB	52.02	49.34	-60.77	2.65

Table 6. Adsorption parameters for the corrosion of mild steel in 1.0 M HCl at different temperatures.

Inhibitor	T (K)	R²	K_{ads} (L/mol)	ΔG_{ads}^0 (kJ/mol)	ΔH_{ads}^0 (kJ/mol)	ΔS_{ads}^0 (J/mol. K)
APAB	303	0.999	16129	34.5	-	-
	303	0.999	16720	-34.6		
PANB	313	0.997	8145	-33.8	-54.5	-66
	323	0.998	4293	-33.2		
	333	0.996	2363	-32.6		

Table 7. Calculated quantum chemical parameters of the inhibitor molecules using B3LYP/6-311++G (d, p).

Inhibitors	E_{HOMO} (eV)	E_{LUMO} (eV)	ΔE_{gap} (eV)	ΔN_{110}
PANB	-6.3508	-2.5371	3.813	0.0985
APAB	-5.4844	-0.6639	4.820	0.3621

Table 8. Fukui indices of PANB and APAB calculated by DFT/6-311++G.

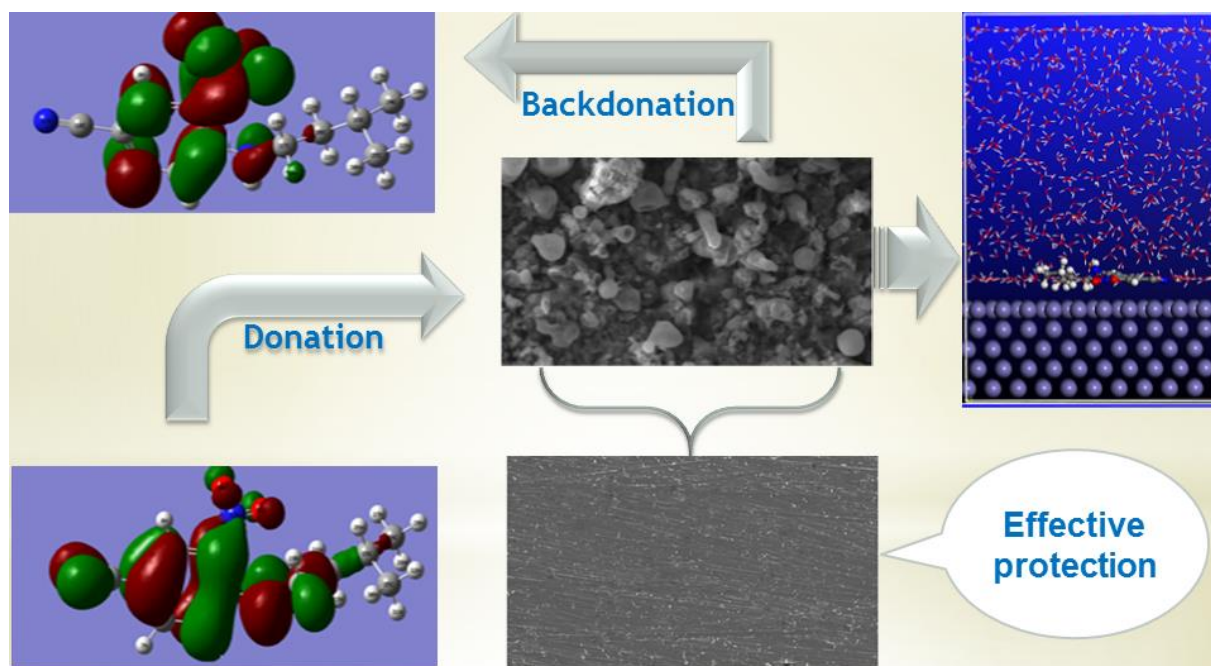
PANB			APAB		
Atom	f_k^+	f_k^-	Atom	f_k^+	f_k^-
C (1)	0.045	0.036	C (1)	0.100	0.057
C (2)	0.015	0.066	C (2)	0.044	0.040
C (3)	0.049	0.045	C (3)	0.070	0.055
C (4)	0.014	0.069	C (4)	0.019	0.055
C (5)	0.041	0.030	C (5)	0.100	0.046
C (6)	0.029	0.069	C (6)	0.037	0.047
H (7)	0.031	0.040	H (7)	0.053	0.044
H (8)	0.041	0.041	H (8)	0.059	0.046
H (9)	0.031	0.048	H (9)	0.048	0.045
C (10)	0.023	0.050	N (10)	0.033	0.109
N (11)	0.041	0.088	H (11)	0.028	0.045
N (12)	0.103	0.014	C (12)	-0.016	-0.025
O (13)	0.216	0.065	C (13)	-0.005	-0.010
O (14)	0.203	0.053	H (14)	0.021	0.038
N (15)	0.040	0.119	H (15)	0.030	0.044
H (16)	0.024	0.046	H (16)	0.010	0.016
C (17)	-0.029	-0.024	H (17)	0.012	0.018
H (18)	0.024	0.051	C (18)	-0.003	-0.004
H (19)	0.025	0.046	C (19)	-0.001	-0.001
C (20)	-0.005	-0.010	C (20)	-0.001	-0.002
H (21)	0.012	0.019	H (21)	0.005	0.007
H (22)	0.011	0.017	H (22)	0.002	0.003
C (23)	-0.003	-0.004	H (23)	0.002	0.003
C (24)	-0.001	-0.001	H (24)	0.003	0.004
C (25)	-0.001	-0.002	H (25)	0.001	0.002
H (26)	0.005	0.008	H (26)	0.002	0.004
H (27)	0.002	0.004	H (27)	0.003	0.005
H (28)	0.002	0.003	N (28)	0.022	0.111
H (29)	0.003	0.005	H (29)	0.019	0.043

H (30)	0.001	0.002	H (30)	0.019	0.043
H (31)	0.002	0.004	C (31)	0.130	0.041
H (32)	0.003	0.005	N (32)	0.154	0.071

ACCEPTED MANUSCRIPT

Table 9. Interaction and binding energies obtained from MD simulations for adsorption of inhibitors on Fe (110) surface.

System	E_{interaction} (KJ/mol)	E_{binding} (KJ/mol)
Fe + PANB + 491H ₂ O + 9Cl ⁻ + 9 H ₃ O ⁺	-495.07	495.07
Fe + APAB + 491H ₂ O + 9Cl ⁻ + 9 H ₃ O ⁺	-328.54	328.54

Graphical Abstract :

ACCEPTED MAI

Highlights

- Novel benzonitrile derivatives have been synthesized and characterized.
- Potentiodynamic polarization curves reveal that tested inhibitors act as mixed type.
- The adsorption of two compounds obeys Langmuir adsorption isotherm.
- Surface morphology was examined by SEM and AFM.
- The experimental results were correlated with DFT and MD simulation results.

ACCEPTED MANUSCRIPT